Accounting for free-surface multiples in Marchenko imaging

Singh, Satyan; Snieder, R; van der Neut, Joost; Thorbecke, Jan Willem; Slob, Evert; Wapenaar, Kees

DOI
10.1190/GEO2015-0646.1

Publication date
2017

Document Version
Final published version

Published in
Geophysics

GEOPHYSICS, VOL. 82, NO. 1 (JANUARY-FEBRUARY 2017); P. R19–R30, 17 FIGS., 3 TABLES.
10.1190/GEO2015-0646.1

Accounting for free-surface multiples in Marchenko imaging

Satyan Singh[1], Roel Snieder[1], Joost van der Neut[2], Jan Thorbecke[2], Evert Slob[2], and Kees Wapenaar[2]

ABSTRACT

Imagine placing a receiver at any location in the earth and recording the response at that location to sources on the surface. In such a world, we could place receivers around our reservoir to better image the reservoir and understand its properties. Realistically, this is not a feasible approach for understanding the subsurface. We have developed an alternative and realizable approach to obtain the response of a buried virtual receiver for sources at the surface. Our method is capable of retrieving the Green's function for a virtual point in the subsurface to the acquisition surface. In our case, a physical receiver is not required at the subsurface point; instead, we require the reflection measurements for sources and receivers at the surface of the earth and a macromodel of the velocity (no small-scale details of the model are necessary). We can interpret the retrieved Green's function as the response to sources at the surface for a virtual receiver in the subsurface. We obtain this Green's function by solving the Marchenko equation, an integral equation pertinent to inverse scattering problems. Our derivation of the Marchenko equation for the Green's function retrieval takes into account the free-surface reflections present in the reflection response (previous work considered a response without free-surface multiples). We decompose the Marchenko equation into up- and downgoing fields and solve for these fields iteratively. The retrieved Green's function not only includes primaries and internal multiples as do previous methods, but it also includes free-surface multiples. We use these up- and downgoing fields to obtain a 2D image of our area of interest, in this case, below a synclinal structure.

INTRODUCTION

Traditionally, to image the subsurface using standard imaging methods, such as reverse time migration (RTM) or Kirchhoff migration, one usually assumes the first-order Born approximation. This assumption only allows us to use the primary reflections in conventional imaging (singly scattered waves). However, without further precautions, the assumption of the first Born approximation leads to artifacts in the presence of multiples. To implement conventional imaging and to ensure the assumption of single scattering holds, one has to remove multiply reflected waves. Multiples consist of internal and free-surface multiples. The removal of free-surface multiples is generally a priority in the recorded reflection response because free-surface multiples are, in general, stronger than internal multiples.

To remove surface multiples from the reflection response, there are model-based methods (Wiggins, 1988; Lokshtanov, 1999), inverse-scattering-based methods (Weglein et al., 1997), data-driven methods (Verschuur et al., 1992; Berkhout and Verschuur, 1997; Ziolkowski et al., 1999; Amundsen, 2001), and recently, inversion methods (van Groenestijn and Verschuur, 2009; Ypma and Verschuur, 2013). The data-driven technique proposed by Verschuur et al. (1992), surface-related multiple elimination (SRME), is a popular method for attenuating multiples because it has been proven to be effective on many real data examples. Although internal multiples are weaker, there are data-driven methods (Berkhout and Verschuur, 1997; Verschuur and Berkhout, 2005) and inverse scattering methods (Ramírez and Weglein, 2005) that remove them from the reflection response. Removing the multiples is not always a simple task; in addition, removal does not allow us to use the valuable

Manuscript received by the Editor 19 November 2015; revised manuscript received 8 July 2016; published online 07 December 2016.
[1]Colorado School of Mines, Department of Geophysics, Center for Wave Phenomena, Golden, Colorado, USA. E-mail: sasingh@mines.edu; rsnieder@mines.edu.
[2]Delft University of Technology, Department of Geoscience and Engineering, Delft, The Netherlands. E-mail: j.r.vanderneut@tudelft.nl; j.w.thorbecke@tudelft.nl; e.c.slob@tudelft.nl; c.p.a.wapenaar@tudelft.nl.

information provided by these multiples. Multiples provide redundant as well as new information that is still useful to improve our image. Using multiples can increase the illumination and lead to better vertical resolution in the image (Schuster et al., 2003; Jiang et al., 2007; Muijs et al., 2007a, 2007b).

A method to use the information embedded in multiples is proposed by Reiter et al. (1991), who use a ray-equation Kirchhoff depth migration to image with free-surface multiple reflections and primaries. In the final image, they achieve extended lateral coverage and an increased signal-to-noise ratio compared with imaging with primaries. However, their method requires reliable separation of free-surface multiples and primaries. In addition, ray-based algorithms, such as that given in Reiter et al. (1991), might fail in complex geologic structures.

One-way wave-equation migration of multiples is proposed by Guitton et al. (2002), Muijs et al. (2007a), and Malcolm et al. (2009) to overcome the shortfalls of ray-based methods. One-way wave-equation migration limits the imaging of steep angle reflectors. Berkhout and Verschuur (2006) modify the principle of SRME to transform multiples into primaries. Accordingly, these new primaries can be subjected to the same imaging criteria as normal primaries. Ong et al. (2002) incorporate reverse time migration (two-way wave equation) into imaging multiples using the source and receiver wavefields as the primary and multiple responses, respectively. Although the subsurface image produced by the modified reverse time migration of multiples gives better illumination and spatial resolution, there are imaging artifacts caused by high-order multiples correlating with the primaries, which place spurious reflectors incorrectly deeper (Ong et al., 2002).

In this paper, we do not investigate the advantages of imaging with multiples; rather, we show that artifacts caused by multiples are largely reduced compared with standard imaging techniques. We propose to use an inverse scattering approach for suppressing artifacts caused by multiples. The physical bases for exact inverse scattering are focusing and time reversal (Rose, 2002a, 2002b), which yield the Marchenko equation. This equation is an integral equation that links the wavefield at any point $\mathbf{x}$ in the medium to the single-sided reflection response.

Broggini et al. (2012) extend the work of Rose (2002a) to geophysics by retrieving the Green's function from reflected waves at the surface. These Green's functions include only primaries and internal multiples (Broggini et al., 2012, 2014) but no surface-related multiples because these authors consider a transparent acquisition boundary. They use the Green's function to image the subsurface (Marchenko imaging), minimizing artifacts produced by internal multiples. We have incorporated the free-surface multiples in the Green's function retrieval algorithm (Singh et al., 2015); therefore, our retrieved Green's functions also include free-surface multiples with the internal multiples and primaries. The major differences between our previous work (Singh et al., 2015) and this work are that (1) we show 2D imaging examples, (2) we use pressure-normalized wavefields compared with flux-normalized wavefields to obtain the Marchenko-type equations, and (3) we solve the Marchenko equations using the f_1 focusing functions (more details on normalized wavefields and focusing functions are given in the "Theory" section). The new focusing functions f_1 directly solve for the up- and downgoing Green's functions, and these Green's functions are used in our imaging scheme.

There is another approach to imaging using inverse scattering proposed by Weglein et al. (2003), who use a nonclosed, or series, solution called the inverse scattering series. Unlike Weglein et al. (2003), our inverse solution to the wave equation is in the form of the Fredholm integral equations of the second kind (Marchenko-type equations).

In this paper, we derive the retrieval of the Green's function by solving Marchenko-type equations using pressure-normalized wavefields. The reason for using pressure-normalized fields is given in the "Theory" section. We show numerical examples of imaging the subsurface using the Green's functions at different depths. Note that the Green's function includes primaries, internal multiples, and free-surface multiples. We call imaging with these Green's functions Marchenko imaging. The distinction between our work and the previous papers of Wapenaar et al. (2014a, 2014b) and Slob et al. (2014) is that we (1) include free-surface multiples in Green's function retrieval, (2) do not require the multiples to be removed from the surface reflection response, and (3) subsequently minimize the artifacts caused by the free-surface multiples in the imaging.

Here, retrieval of the Green's function and hence the Marchenko imaging is an acoustic technique; however, da Costa Filho et al. (2014), da Costa Filho and Curtis (2015), Wapenaar (2014), and Wapenaar and Slob (2014) extend the procedures to elastic data without free-surface multiples.

THEORY

Retrieving Green's function in the presence of a free surface, using the Marchenko-type equations, is derived in multiple dimensions by Singh et al. (2015), but their numerical examples are in 1D. The reflection response R that Singh et al. (2015) use to retrieve these functions is flux normalized, which facilitates the derivation of the 3D Marchenko equations (Wapenaar et al., 2014a). Similarly, the retrieval of Green's function without a free surface also uses flux-normalized wavefields (Broggini et al., 2012; Wapenaar et al., 2013). However, the Green's function retrieval is not restricted to flux-normalized fields and can be modified to pressure-normalized fields. Wapenaar et al. (2014a) derive the retrieval of the Green's function using pressure-normalized fields in the absence of a free surface.

In this paper, we demonstrate an alternative approach to Singh et al. (2015) by using pressure-normalized fields to retrieve the Green's function in the presence of a free surface. Like previous papers on Green's function retrieval, we obtain these Green's functions by solving Marchenko-type equations (Slob et al., 2014; Wapenaar et al., 2014b). We show 2D numerical examples of the retrieval and its application to imaging the subsurface. More details on flux- and pressure-normalized wavefields can be obtained from Ursin (1983) and Wapenaar and Grimbergen (1996).

Acoustic pressure p and vertical particle velocity v_3 are related to any type of one-way normalized fields (downgoing p^+ and upgoing p^-) in the space-frequency domain according to

$$\begin{pmatrix} p \\ v_3 \end{pmatrix} = \begin{pmatrix} \mathcal{L}_1 & \mathcal{L}_1 \\ \mathcal{L}_2 & -\mathcal{L}_2 \end{pmatrix} \begin{pmatrix} p^+ \\ p^- \end{pmatrix}; \tag{1}$$

conversely, the p^+ and p^- are related to p and v_3 by

$$\begin{pmatrix} p^+ \\ p^- \end{pmatrix} = \frac{1}{2}\begin{pmatrix} \mathcal{L}_1^{-1} & \mathcal{L}_2^{-1} \\ \mathcal{L}_1^{-1} & -\mathcal{L}_2^{-1} \end{pmatrix}\begin{pmatrix} p \\ v_3 \end{pmatrix}. \tag{2}$$

Here, $\mathcal{L}_1$, $\mathcal{L}_2$, and their inverses are pseudodifferential operators (Wapenaar, 1998). For pressure normalization, $\mathcal{L}_1 = \mathcal{I}$ (identity operator), whereas for flux normalization, equation 2 becomes

$$\begin{pmatrix} p^+ \\ p^- \end{pmatrix} = \begin{pmatrix} \mathcal{L}_2^t & \mathcal{L}_1^t \\ \mathcal{L}_2^t & -\mathcal{L}_1^t \end{pmatrix}\begin{pmatrix} p \\ v_3 \end{pmatrix}, \tag{3}$$

where superscript t denotes operator transposition.

In a laterally invariant medium, equations 1 and 2 become, in the wavenumber-frequency domain,

$$\begin{pmatrix} \tilde{p} \\ \tilde{v}_3 \end{pmatrix} = \begin{pmatrix} \tilde{\mathcal{L}}_1 & \tilde{\mathcal{L}}_1 \\ \tilde{\mathcal{L}}_2 & -\tilde{\mathcal{L}}_2 \end{pmatrix}\begin{pmatrix} \tilde{p}^+ \\ \tilde{p}^- \end{pmatrix}, \tag{4}$$

and

$$\begin{pmatrix} \tilde{p}^+ \\ \tilde{p}^- \end{pmatrix} = \frac{1}{2}\begin{pmatrix} \tilde{\mathcal{L}}_1^{-1} & \tilde{\mathcal{L}}_2^{-1} \\ \tilde{\mathcal{L}}_1^{-1} & -\tilde{\mathcal{L}}_2^{-1} \end{pmatrix}\begin{pmatrix} \tilde{p} \\ \tilde{v}_3 \end{pmatrix}, \tag{5}$$

retrospectively. Here, $\tilde{\mathcal{L}}_1$, $\tilde{\mathcal{L}}_2$, and their inverses are scalar functions (not operators). Equations 4 and 5 hold for any type of normalization. For pressure normalization, we have $\tilde{\mathcal{L}}_1 = 1$ and $\tilde{\mathcal{L}}_2 = k_3/\omega\rho$, where $k_3 = \sqrt{\omega^2/c^2 - |\mathbf{k}|^2}$, with $\mathbf{k} = (k_1, k_2)$. For flux normalization, we have $\tilde{\mathcal{L}}_1 = \sqrt{\omega\rho/2k_3}$ and $\tilde{\mathcal{L}}_2 = \sqrt{k_3/2\omega\rho}$.

We use pressure-normalized wavefields because the relationship between the two-way Green's function and the pressure-normalized one-way Green's functions is more straightforward than with flux normalization. The sum of the one-way pressure-normalized fields is equal to the pressure. The flux-normalized up- and downgoing Green's functions $\bar{G}^+$ and $\bar{G}^-$ are related in the space domain to the two-way Green's function by (equation 1)

$$G = \mathcal{L}_1(x_{3,i})\mathcal{L}_1(x_{3,0})(\bar{G}^+ + \bar{G}^-), \tag{6}$$

where $\mathcal{L}_1(x_{3,0})$ and $\mathcal{L}_1(x_{3,i})$ are the operators at the depth levels $x_3 = x_{3,0}$ and $x_3 = x_{3,i}$, respectively.

Therefore, to obtain the two-way Green's function of the pressure recording for a source of volume-injection type using flux-normalized one-way wavefields, one must apply $\mathcal{L}_1$ at $x_3 = x_{3,0}$ and $x_3 = x_{3,i}$ to the sum of $\bar{G}^+$ and $\bar{G}^-$. However, to obtain this same two-way Green's function using pressure-normalized wavefields, we add the up- and downgoing retrieved Green's functions. Although the pressure-normalized wavefields are simpler to obtain compared with flux-normalized wavefields, their use in the derivation of the retrieval of the Green's function is more involved.

We begin the derivation of the Green's function retrieval with the frequency-domain one-way reciprocity theorems of the convolution and correlation types (Slob et al., 2014; Wapenaar et al., 2014a), which hold for lossless media between ∂D_0 (acquisition surface) and ∂D_i (arbitrary depth level):

$$\begin{aligned}\int_{\partial D_0} \rho^{-1}(\mathbf{x})[(\partial_3 p_A^+)p_B^- + (\partial_3 p_A^-)p_B^+]d\mathbf{x_0} \\ = -\int_{\partial D_i} \rho^{-1}(\mathbf{x})[p_A^+(\partial_3 p_B^-) + p_A^-(\partial_3 p_B^+)]d\mathbf{x_i},\end{aligned} \tag{7}$$

$$\begin{aligned}\int_{\partial D_0} \rho^{-1}(\mathbf{x})[(\partial_3 p_A^+)^* p_B^+ + (\partial_3 p_A^-)^* p_B^-]d\mathbf{x_0} \\ = -\int_{\partial D_i} \rho^{-1}(\mathbf{x})[(p_A^+)^*(\partial_3 p_B^+) + (p_A^-)^*(\partial_3 p_B^-)]d\mathbf{x_i}.\end{aligned} \tag{8}$$

The asterisk * denotes complex conjugation, and the subscripts A and B denote two wave states. Equations 7 and 8 are the reciprocity theorems for pressure-normalized one-way wavefields. Equation 8 does not account for evanescent and horizontally propagating waves, such as surface waves and horizontally diffracted waves; hence, the presence of these waves in our fields ($p_A^\pm$ and $p_B^\pm$) can introduce artifacts in our solutions. The spatial coordinates are defined by their horizontal and depth components; for instance $\mathbf{x_0} = (\mathbf{x_{H,0}}, x_{3,0})$, where $\mathbf{x_{H,0}}$ are the horizontal coordinates at a depth $x_{3,0}$. These one-way reciprocity theorems hold for up- and downgoing pressure-normalized fields.

One-way wavefields

The reciprocity theorems are used to solve for the Green's function. We define the Green's function as the response to an impulsive point source of the volume injection rate at $\mathbf{x_0''}$ just above ∂D_0. This Green's function obeys the scalar wave equation

$$\rho\nabla.\left(\frac{1}{\rho}\nabla G\right) - \frac{1}{c^2}\frac{\partial^2 G}{\partial t^2} = -\rho\delta(\mathbf{x} - \mathbf{x_0''})\frac{\partial\delta(t)}{\partial t}. \tag{9}$$

We include the time derivative on the right side because we consider the source to be of the volume injection rate. Using the Fourier convention $p(\mathbf{x},\omega) = \int_{-\infty}^{\infty} p(\mathbf{x},t)\exp(-j\omega t)dt$ in the frequency domain, equation 9 becomes

$$\rho\nabla.\left(\frac{1}{\rho}\nabla G\right) + \frac{\omega^2}{c^2}G = -j\omega\rho\delta(\mathbf{x} - \mathbf{x_0''}). \tag{10}$$

Because we are using one-way reciprocity theorems, equations 7 and 8, we define our Green's function (two-way) as a sum of the up- and downgoing pressure-normalized one-way Green's functions:

$$G(\mathbf{x}, \mathbf{x_0''}, \omega) = G^{+,q}(\mathbf{x}, \mathbf{x_0''}, \omega) + G^{-,q}(\mathbf{x}, \mathbf{x_0''}, \omega), \tag{11}$$

where $\mathbf{x}$ is the observation point. Defined this way, the one-way Green's functions are decomposed at the observation point $\mathbf{x}$ denoted by the first superscripts + or −. We consider downward to be positive; hence, the superscript + represents downgoing waves, and − represents upgoing waves. The second superscript (q) refers to the volume-rate injection source at $\mathbf{x_0''}$. For instance, $G^{-,q}(\mathbf{x}, \mathbf{x_0''}, \omega)$ is the pressure-normalized upgoing Green's function at $\mathbf{x}$ due to a volume injection source at $\mathbf{x_0''}$ in the frequency domain.

Similar to equation A-11 in Wapenaar et al. (2014a), we define the vertical derivative of the upgoing Green's function at the acquisition surface ∂D_0, just below the free surface, as

$$\partial_3 G^{-,q}(\mathbf{x}, \mathbf{x_0''}, \omega)|_{x_3 = x_{3,0}} = \frac{1}{2}j\omega\rho(\mathbf{x_0})R(\mathbf{x_0''}, \mathbf{x_0}, \omega). \tag{12}$$

However, in our case, $\partial_3 G^{-,q}$ and R include free-surface multiples. Considering the downward component of the source and the surface-reflected waves, we define

$$\partial_3 G^{+,q}(\mathbf{x}, \mathbf{x}_0'', \omega)|_{x_3=x_{3,0}} = -\frac{1}{2} j\omega\rho(\mathbf{x}_0)[\delta(\mathbf{x}_H - \mathbf{x}_H'') + rR(\mathbf{x}_0'', \mathbf{x}_0, \omega)], \quad (13)$$

where r denotes the reflection coefficient of the free surface (in the simple examples shown in this paper, r is -1). For the downgoing field $\partial_3 G^{+,q}$, at and below ∂D_0, we consider the downward component of the source $-1/2 j\omega\rho(\mathbf{x_0})\delta(\mathbf{x_H} - \mathbf{x_H''})$ and the reflections from the free surface $-1/2 j\omega\rho(\mathbf{x_0})rR(\mathbf{x_0''}, \mathbf{x_0}, \omega)$, similar to the Marchenko derivation with flux-normalized fields from Singh et al. (2015). At ∂D_i, the up- and downgoing waves are $G^{-,q}$ and $G^{+,q}$, respectively. We define state A, shown in Figure 1, as the one-way pressure-normalized wavefields in the actual medium $p_A^{\pm}$ at ∂D_0 and ∂D_i, as shown in Table 1.

Similar to the previous papers that derive Marchenko-type equations (Wapenaar et al., 2013, 2014a; Slob et al., 2014; Singh et al., 2015), we also define focusing functions as state B (see Figure 2). The focusing function f_1 is a solution of the sourceless wave equation for the waves that focus at a point at the bottom of the truncated medium. The truncated reference medium is reflection free above ∂D_0 and below ∂D_i, but it is the same as the actual medium between ∂D_0 and ∂D_i (see Figure 2). The f_1 function is defined as waves that focus at $\mathbf{x}_i'$ at a defined depth level (∂D_i) for incoming f_1^+ and outgoing f_1^- waves at the acquisition surface (∂D_0) $\mathbf{x_0}$ (Figure 2).

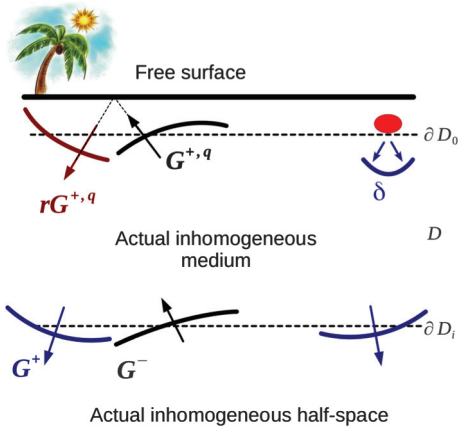

Figure 1. The one-way Green's functions in the actual inhomogeneous medium in the presence of a free surface at the acquisition surface ∂D_0 and the arbitrary surface ∂D_i. The tree indicates the presence of the free surface.

Table 1. The pressure-normalized one-way wavefields in the actual inhomogeneous medium in the presence of a free surface at the depth level ∂D_0 and ∂D_i. Here $p_A^{\pm}$ symbolizes one-way wavefields at arbitrary depth levels in the inhomogeneous medium, whereas r is the reflection coefficient of the free surface.

∂D_0	$\partial_3 p_A^+ = \partial_3 G^{+,q}(\mathbf{x_0}, \mathbf{x_0''}, \omega) = -\frac{1}{2} j\omega\rho(\mathbf{x_0})(\delta(\mathbf{x_H} - \mathbf{x_H''}) + rR(\mathbf{x_0''}, \mathbf{x_0}, \omega))$
	$\partial_3 p_A^- = \partial_3 G^{-,q}(\mathbf{x_0}, \mathbf{x_0''}, \omega) = \frac{1}{2} j\omega\rho(\mathbf{x_0})R(\mathbf{x_0''}, \mathbf{x_0}, \omega)$
∂D_i	$p_A^+ = G^{+,q}(\mathbf{x_i}, \mathbf{x_0''}, \omega)$
	$p_A^- = G^{-,q}(\mathbf{x_i}, \mathbf{x_0''}, \omega)$

The one-way wavefields for the f_1 function at the depth levels ∂D_0 and ∂D_i, which we define as state B, are shown in Figure 2 and Table 2. The one-way focusing function $f_1^+(\mathbf{x}, \mathbf{x_i'}, t)$ is shaped such that $f_1(\mathbf{x}, \mathbf{x_i'}, t)$ focuses at $\mathbf{x_i'}$ at $t = 0$. At the focusing point $\mathbf{x_i'}$ of f_1, we define $\partial_3 f_1(\mathbf{x}, \mathbf{x_i'}, t)$ as $-1/2\rho(\mathbf{x_i'})\delta(\mathbf{x}_H - \mathbf{x}_H')\partial\delta(t)/\partial t$, a 2D and 1D Dirac delta function in space and time, respectively. After the focusing point, $f_1(\mathbf{x}, \mathbf{x_i'}, t)$ continues to diverge as a downgoing field $f_1^+(\mathbf{x}, \mathbf{x_i'}, t)$ into the reflection-free reference half-space (Wapenaar et al., 2014a).

By substituting the one-way wavefields given in Table 1 (state A) and Table 2 (state B) into the convolution reciprocity theorem, equation 7, we get the upgoing Green's function

$$G^{-,q}(\mathbf{x_i'}, \mathbf{x_0''}, \omega) = \int_{\partial D_0} [f_1^+(\mathbf{x_0}, \mathbf{x_i'}, \omega)R(\mathbf{x_0''}, \mathbf{x_0}, \omega) - rf_1^-(\mathbf{x_0}, \mathbf{x_i'}, \omega)R(\mathbf{x_0''}, \mathbf{x_0}, \omega)]d\mathbf{x_0} - f_1^-(\mathbf{x_0''}, \mathbf{x_i'}, \omega). \quad (14)$$

Likewise, substituting the one-way wavefields in Tables 1 and 2 into the correlation reciprocity theorem, equation 8, we get the downgoing Green's function:

$$G^{+,q}(\mathbf{x_i'}, \mathbf{x_0''}, \omega) = -\int_{\partial D_0} [f_1^-(\mathbf{x_0}, \mathbf{x_i'}, \omega)^* R(\mathbf{x_0''}, \mathbf{x_0}, \omega) - rf_1^+(\mathbf{x_0}, \mathbf{x_i'}, \omega)^* R(\mathbf{x_0''}, \mathbf{x_0}, \omega)]d\mathbf{x_0} + f_1^+(\mathbf{x_0''}, \mathbf{x_i'}, \omega)^*. \quad (15)$$

Equations 14 and 15 are identical to the equations for G^- and G^+ of Singh et al. (2015); however, our Green's functions are pressure normalized. In addition, unlike Singh et al. (2015), there is no need to use equation 6 to obtain the two-way Green's function; one can use equation 11 to get G. Equations 14 and 15 are the starting point for deriving the 3D Marchenko-type equations.

Marchenko's equations

Equations 14 and 15 are two equations for four unknowns ($G^{+,q}, G^{-,q}, f_1^+$, and f_1^-). After an inverse Fourier transform, we can separate these equations into two temporal parts: times earlier than the first arrival and times later than the first arrival of the Green's function at the virtual receiver location. We consider $t_d(\mathbf{x_i'}, \mathbf{x_0''})$ to be the first-arrival time of the Green's function. Hence, we can separate equations 14 and 15 for $t \geq t_d$ and $t < t_d$. These temporal constraints, along with the causality requirements, give rise to two equations and two unknowns for $f_1^{\pm}$, after which we can retrieve $G^{\pm,q}$ by substitution into equations 14 and 15.

An estimate of the first-arrival time $t_d(\mathbf{x_i'}, \mathbf{x_0''})$ is, for example, obtained by using finite-difference modeling of the waveforms in a smooth velocity model that acts as a macromodel. Evaluating equations 14 and 15 for times before t_d yields

$$f_1^-(\mathbf{x_0''}, \mathbf{x_i'}, t) = \int_{\partial D_0} d\mathbf{x_0} \int_{-\infty}^{t} [f_1^+(\mathbf{x_0}, \mathbf{x_i'}, t') \times R(\mathbf{x_0''}, \mathbf{x_0}, t - t') - rf_1^-(\mathbf{x_0}, \mathbf{x_i'}, t') \times R(\mathbf{x_0''}, \mathbf{x_0}, t - t')]dt', \quad (16)$$

$$f_1^+(\mathbf{x_0''},\mathbf{x_i'},-t)=\int_{\partial D_0}d\mathbf{x_0}\int_{-\infty}^{t}[f_1^-(\mathbf{x_0},\mathbf{x_i'},-t')R(\mathbf{x_0''},\mathbf{x_0},t-t')-rf_1^+(\mathbf{x_0},\mathbf{x_i'},-t')R(\mathbf{x_0''},\mathbf{x_0},t-t')]dt', \quad (17)$$

because causality dictates that $G^{\pm,q}$ vanish for $t<t_d(\mathbf{x_i'},\mathbf{x_0''})$.

In the reference medium in which the focusing functions exist, we can define up- and downgoing waves with respect to transmission responses $T(\mathbf{x_0},\mathbf{x_i'},t)$ at arbitrary depth levels (state C), as shown in Figure 3. Hence, $T(\mathbf{x_0},\mathbf{x_i'},t)$ is the transmission in the reference medium that is the actual inhomogeneous medium between ∂D_0 and ∂D_i, but it is homogeneous above and below ∂D_0 and ∂D_i.

The up- and downgoing waves in Figure 3 are defined in Table 3 according to the reciprocity relations.

Substituting the one-way wavefields represented in Tables 2 and 3 into the one-way convolution reciprocity theorem, equation 7 yields

$$\delta(\mathbf{x_H''}-\mathbf{x_H'})=\int_{\partial D_0}\frac{\partial_3 T(\mathbf{x_0},\mathbf{x_i'},\omega)}{-\frac{1}{2}j\omega\rho(\mathbf{x_0})}f_1^+(\mathbf{x_0},\mathbf{x_i''},\omega)d\mathbf{x_0}, \quad (18)$$

where we represent the source positions of the focusing function f_1^+ with double primes instead of single primes. For simplicity, we define $\mathcal{T}(\mathbf{x_0},\mathbf{x_i'},\omega)=(\partial_3 T(\mathbf{x_0},\mathbf{x_i'},\omega))/(-1/2j\omega\rho(\mathbf{x_0}))$; hence, in the time domain (from equation 18), f_1^+ is the inverse of the transmission response:

$$f_1^+(\mathbf{x_0},\mathbf{x_i'},t)=\mathcal{T}^{\text{inv}}(\mathbf{x_0},\mathbf{x_i'},t). \quad (19)$$

Analogous to Wapenaar et al. (2014b), Slob et al. (2014), and Singh et al. (2015), we adopt the assumption for the pressure-normalized version of f_1^+ to be

$$f_1^+(\mathbf{x_0},\mathbf{x_i'},t)=\mathcal{T}_d^{\text{inv}}(\mathbf{x_0},\mathbf{x_i'},t)+M(\mathbf{x_0},\mathbf{x_i'},t), \quad (20)$$

where $\mathcal{T}_d^{\text{inv}}$ is the inverse of the direct arrival of the transmission response and M is the coda following $\mathcal{T}_d^{\text{inv}}$. We can approximate $\mathcal{T}_d^{\text{inv}}$ as the time-reversed direct arrival of the pressure-normalized Green's function (hence the need for a smooth velocity model as previously mentioned).

Substituting assumption 20 into the time-domain representation of equations 16 and 17 yields the following Marchenko equations for $t<t_d(\mathbf{x_i'},\mathbf{x_0''})$:

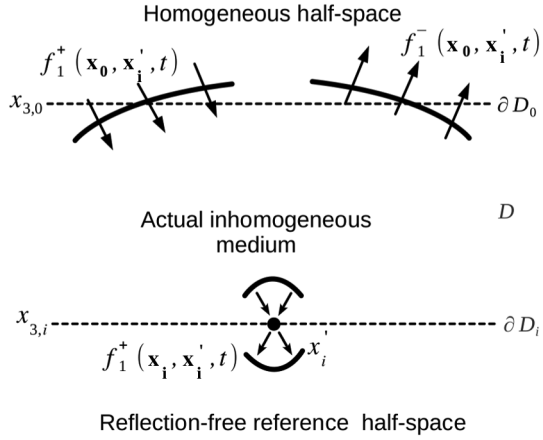

Figure 2. Focusing function f_1 that focuses at $\mathbf{x_i'}$ in the reference medium, in which above ∂D_0 is homogeneous and below ∂D_i is reflection free.

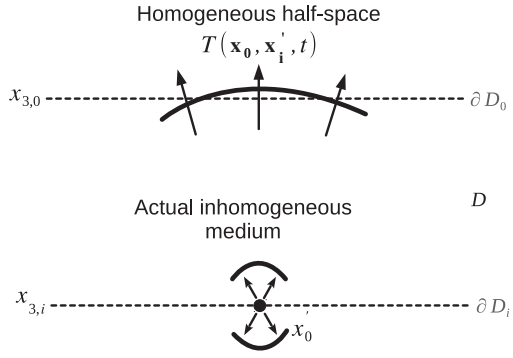

Figure 3. The transmission response $T(\mathbf{x_0},\mathbf{x_i'},t)$ in the reference configuration.

Table 2. The one-way wavefields of the focusing function f_1 at the acquisition surface ∂D_0 and the level in which f_1 focuses ∂D_i. Here $p_B^{\pm}$ symbolizes one-way wavefields in the frequency domain at arbitrary depth levels in the truncated reference medium (see Figure 2).

∂D_0	$p_B^+ = f_1^+(\mathbf{x_0},\mathbf{x_i'},\omega)$
	$p_B^- = f_1^-(\mathbf{x_0},\mathbf{x_i'},\omega)$
∂D_i	$\partial_3 p_B^+ = \partial_3 f_1^+(\mathbf{x_i},\mathbf{x_i'},\omega) = -\frac{1}{2}j\omega\rho(\mathbf{x_i'})\delta(\mathbf{x}_H-\mathbf{x}_H')$
	$\partial_3 p_B^- = \partial_3 f_1^-(\mathbf{x_i},\mathbf{x_i'},\omega)$

Table 3. The one-way wavefields in the reference medium at the acquisition surface ∂D_0 and the level in which f_1 focuses ∂D_i. Here $p_C^{\pm}$ symbolizes one-way wavefields in the frequency domain at arbitrary depth levels in the reference medium (see Figure 3). The source location is just below ∂D_i.

∂D_0	$\partial_3 p_C^+ = 0$
	$\partial_3 p_C^- = \partial_3 T(\mathbf{x_0},\mathbf{x_i'},\omega)$
∂D_i	$p_C^+ = 0$
	$p_C^- = \delta(\mathbf{x}_H-\mathbf{x}_H')$

$$
\begin{aligned}
&f_1^-(\mathbf{x_0''},\mathbf{x_i'},t)\\
&\quad=\int_{\partial D_0} d\mathbf{x_0}\int_{-\infty}^{-t_d^\epsilon(\mathbf{x_i'},\mathbf{x_0})}\mathcal{T}_d^{\text{inv}}(\mathbf{x_0},\mathbf{x_i'},t')R(\mathbf{x_0''},\mathbf{x_0},t-t')dt'\\
&\quad+\int_{\partial D_0} d\mathbf{x_0}\int_{-t_d^\epsilon(\mathbf{x_i'},\mathbf{x_0})}^{t} M(\mathbf{x_0},\mathbf{x_i'},t')R(\mathbf{x''}_0,\mathbf{x_0},t-t')dt'\\
&\quad-r\int_{\partial D_0} d\mathbf{x_0}\int_{-t_d^\epsilon(\mathbf{x_i'},\mathbf{x_0})}^{t} f_1^-(\mathbf{x_0},\mathbf{x_i'},t')R(\mathbf{x''}_0,\mathbf{x_0},t-t')]dt',
\end{aligned}
\tag{21}
$$

$$
\begin{aligned}
&M(\mathbf{x_0''},\mathbf{x_i'},-t)\\
&\quad=\int_{\partial D_0} d\mathbf{x_0}\int_{-t_d^\epsilon(\mathbf{x_i'},\mathbf{x_0})}^{t} f_1^-(\mathbf{x_0},\mathbf{x_i'},-t')R(\mathbf{x_0''},\mathbf{x_0},t-t')dt'\\
&\quad-r\int_{\partial D_0} d\mathbf{x_0}\int_{-t_d^\epsilon(\mathbf{x_i'},\mathbf{x_0})}^{\infty} M(\mathbf{x_0},\mathbf{x_i'},t')R(\mathbf{x_0''},\mathbf{x_0},t+t')]dt'\\
&\quad-r\int_{\partial D_0} d\mathbf{x_0}\int_{-t}^{-t_d^\epsilon(\mathbf{x_i'},\mathbf{x_0})}\mathcal{T}_d^{\text{inv}}(\mathbf{x_0},\mathbf{x_i'},t')R(\mathbf{x_0''},\mathbf{x_0},t+t')]dt',
\end{aligned}
\tag{22}
$$

with $t_d^\epsilon(\mathbf{x_i'},\mathbf{x_0}) = t_d(\mathbf{x_i'},\mathbf{x_0}) - \epsilon$, where ϵ is a small positive constant to include the direct arrival in the integrals. We choose to solve the Marchenko equations 21 and 22 iteratively as follows:

$$
\begin{aligned}
&f_{1,k}^-(\mathbf{x_0''},\mathbf{x_i'},t)\\
&\quad=\int_{\partial D_0} d\mathbf{x_0}\int_{-\infty}^{-t_d^\epsilon(\mathbf{x_i'},\mathbf{x_0})}\mathcal{T}_d^{\text{inv}}(\mathbf{x_0},\mathbf{x_i'},t')R(\mathbf{x_0''},\mathbf{x_0},t-t')dt'\\
&\quad+\int_{\partial D_0} d\mathbf{x_0}\int_{-t_d^\epsilon(\mathbf{x_i'},\mathbf{x_0})}^{t} M_{k-1}(\mathbf{x_0},\mathbf{x_i'},t')R(\mathbf{x_0''},\mathbf{x_0},t-t')dt'\\
&\quad-r\int_{\partial D_0} d\mathbf{x_0}\int_{-t_d^\epsilon(\mathbf{x_i'},\mathbf{x_0})}^{t} f_{1,k-1}^-(\mathbf{x_0},\mathbf{x_i'},t')R(\mathbf{x_0''},\mathbf{x_0},t-t')]dt',
\end{aligned}
\tag{23}
$$

$$
\begin{aligned}
&M_k(\mathbf{x_0''},\mathbf{x_i'},-t)\\
&\quad=\int_{\partial D_0} d\mathbf{x_0}\int_{-t_d^\epsilon(\mathbf{x_i'},\mathbf{x_0})}^{t} f_{1,k}^-(\mathbf{x_0},\mathbf{x_i'},-t')R(\mathbf{x_0''},\mathbf{x_0},t-t')dt'\\
&\quad-r\int_{\partial D_0} d\mathbf{x_0}\int_{-t_d^\epsilon(\mathbf{x_i'},\mathbf{x_0})}^{\infty} M_{k-1}(\mathbf{x_0},\mathbf{x_i'},t')R(\mathbf{x_0''},\mathbf{x_0},t+t')]dt'\\
&\quad-r\int_{\partial D_0} d\mathbf{x_0}\int_{-t}^{-t_d^\epsilon(\mathbf{x_i'},\mathbf{x_0})}\mathcal{T}_d^{\text{inv}}(\mathbf{x_0},\mathbf{x_i'},t')R(\mathbf{x_0''},\mathbf{x_0},t+t')]dt'.
\end{aligned}
\tag{24}
$$

Note that we are not limited to solving the Marchenko equations iteratively; one can use a preferred integral solver such as conjugate gradients or least-squares inversion. The corresponding focusing function f_1^+ for each iteration reads (from equation 19),

$$
f_{1,k}^+(\mathbf{x_0},\mathbf{x_i'},t) = \mathcal{T}_d^{\text{inv}}(\mathbf{x_0},\mathbf{x_i'},t) + M_{k-1}(\mathbf{x_0},\mathbf{x_i'},t). \tag{25}
$$

Marchenko iterative scheme

We initialize the Marchenko iterative scheme by obtaining the direct arrival of Green's function. The time-reversed version of this direct arrival can be used as an approximation for $\mathcal{T}_d^{\text{inv}}$ that takes into account traveltimes and geometric spreading but ignores transmission losses at the interfaces (Wapenaar et al., 1989, 2014a).

With this initialization, the iterative scheme for $k = 0$ is as follows:

$$
\begin{aligned}
f_{1,0}^-(\mathbf{x_0''},\mathbf{x_i'},-t) = &\int_{\partial D_0} d\mathbf{x_0}\int_{-\infty}^{-t_d^\epsilon(\mathbf{x_i'},\mathbf{x_0})}\mathcal{T}_d^{\text{inv}}(\mathbf{x_0},\mathbf{x_i'},t')\\
&\times R(\mathbf{x_0''},\mathbf{x_0},t-t')dt',
\end{aligned}
\tag{26}
$$

$$
\begin{aligned}
&M_0(\mathbf{x_0''},\mathbf{x_i'},-t)\\
&\quad=\int_{\partial D_0} d\mathbf{x_0}\int_{-t_d^\epsilon(\mathbf{x_i'},\mathbf{x_0})}^{t} f_{1,0}^-(\mathbf{x_0},\mathbf{x_i'},-t')R(\mathbf{x_0''},\mathbf{x_0},t-t')dt'\\
&\quad-r\int_{\partial D_0} d\mathbf{x_0}\int_{-t}^{-t_d^\epsilon(\mathbf{x_i'},\mathbf{x_0})}\mathcal{T}_d^{\text{inv}}(\mathbf{x_0},\mathbf{x_i'},t')R(\mathbf{x_0''},\mathbf{x_0},t+t')]dt'.
\end{aligned}
\tag{27}
$$

Now the iterative scheme described in equations 23–25 can be initiated with equations 26 and 27 to solve for f_1^+ and f_1^-. These focusing functions can then be substituted in equations 11, 14, and 15 to obtain the retrieved two-way pressure-normalized Green's function, and the up- and downgoing one-way pressure-normalized Green's function, respectively.

Marchenko imaging

Broggini et al. (2012, 2014), Behura et al. (2014), Wapenaar et al. (2011, 2014b), Slob et al. (2014), and Singh et al. (2015) have all used the retrieved one-way Green's functions to produce an image. Marchenko imaging is built on the concept of obtaining the reflection response from the up- and downgoing wavefields at an arbitrary depth level. The use of up- and downgoing wavefields for imaging is not a new principle. Claerbout (1971), Wapenaar et al. (2000), and Amundsen (2001) show that one can get the reflection response below an arbitrary depth level once the up- and downgoing wavefields are available.

The governing equation for imaging with such one-way wavefields is (Wapenaar et al., 2008)

$$
\begin{aligned}
G^{-,q}(\mathbf{x_i'},\mathbf{x_0''},t) = &\int_{\partial D_i} d\mathbf{x_i}\int_{-\infty}^{\infty} G^{+,q}(\mathbf{x_i},\mathbf{x_0''},t-t')\\
&\times R_0(\mathbf{x_i'},\mathbf{x_i},t')dt',
\end{aligned}
\tag{28}
$$

where ∂D_i is an arbitrary depth level and R_0 is the reflection response of the medium below ∂D_i. Note that equation 28 holds for outgoing and incoming wavefields normal to the surface ∂D_i. However, the retrieved Green's functions (current methods) are strictly up- and downgoing wavefields at arbitrary depth levels, which correspond to a flat surface ∂D_i. The reflection response R_0, in equation 28, is the response as if everything above ∂D_i is transparent. Therefore, R_0 is a virtual reflection response as if there were receivers and sources at ∂D_i, in the absence of a free surface at ∂D_i.

Significantly, the response R_0 is blind to the actual overburden above ∂D_i. Wapenaar et al. (2014b) have shown the retrieval of this virtual reflection below a complex overburden. In this paper, any variable with a subscript 0 (e.g., R_0) indicates that no free surface is present.

We choose to solve for R_0 in equation 28 by multidimensional deconvolution (van der Neut et al., 2011). Details of solving equation 28 using retrieved Green's functions are given in Wapenaar et al. (2014b). The significant difference between our work and the previous Marchenko imaging papers is that our Green's functions include information of the actual medium with the free surface and include all (free surface and internal) multiples. This corresponds to minimizing the artifacts caused by free-surface multiples and internal multiples in the imaging. Once we obtain R_0 at each image point, our subsurface image is the contribution of R_0 at zero offset and zero time, i.e., $R_0(\mathbf{x_i}, \mathbf{x_i}, 0)$.

NUMERICAL EXAMPLES

Our numerical model has variable velocity and density, as shown in Figures 4 and 5, respectively. We use a 2D inhomogeneous subsurface model with a syncline structure. The horizontal range of the model is −3000 to 3000 m. Our goal is to show (1) the retrieval of Green's function $G(\mathbf{x}_i', \mathbf{x}_0'', t)$ for a virtual receiver at $\mathbf{x_i} = (0, 1100)$ m and the corresponding variable source locations at $\mathbf{x}_0''$ and (2) the subsurface image below the syncline structure. To obtain Green's function, we need the pressure-normalized reflection response $R(\mathbf{x}_0'', \mathbf{x_0}, \omega)$ and a macromodel (no small-scale details of the model are necessary). The reflection response is computed by finite differences with vertical-force sources and particle velocity receiver recordings, at the surface. The receiver spacing is 10 m, and the source is a Ricker wavelet with a central frequency of 20 Hz. We use this finite-difference response and equation 2 to get the pressure-normalized reflection response $R(\mathbf{x}_0'', \mathbf{x_0}, \omega)$ that we deconvolve with the source wavelet. See Figure 6 for an example of a single shot at $\mathbf{x}_0'' = (0, 0)$ m with the direct arrivals from source to receivers removed. The macromodel is a smooth version of the velocity model that we use to compute the traveltimes of the direct arrival (see Figure 7). No density information is required.

We use the macromodel to obtain the first arrival from the virtual source at $\mathbf{x_i} = (0, 1100)$ m to the surface (by an eikonal solver). This first arrival is time reversed to initialize the iterative scheme with $\mathcal{T}_d^{\text{inv}}$ as well as to guide us in choosing the time windows for equations 14–17. Figure 8 shows $\mathcal{T}_d^{\text{inv}}$ that is equivalent to $f_{1,0}^{+}$.

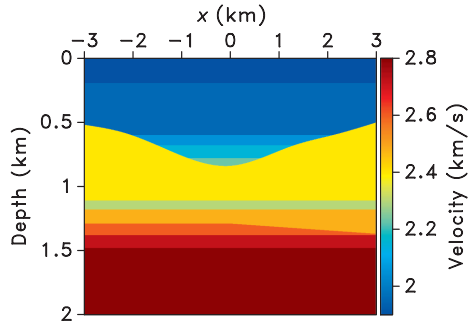

Figure 4. The velocity model ranging from velocities 1.9 to 2.8 km/s as shown in the color bar.

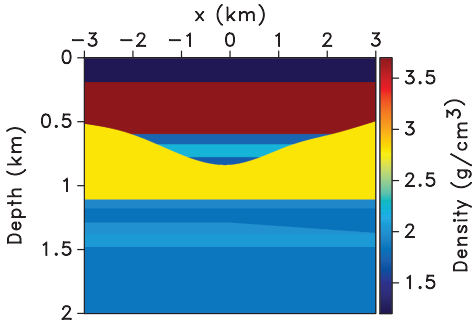

Figure 5. The density model ranging from densities 1 to 3.5 g/cm^3 as shown in the color bar.

Focusing functions

We build the focusing functions $f_{1,k}^{+}$ and $f_{1,k}^{-}$ using the iterative scheme in equations 23–25. Figure 9 shows the functions $f_{1,k}^{+}$ and $f_{1,k}^{-}$ for iteration index $k = 0, 1, 5$. Note that these one-way focusing functions reside in the time window $-t_d < t < t_d$.

The integrals that we use to solve for the focusing function, equations 16 and 17, have spatial limits between $-\infty$ and ∞, which means that we require an infinite aperture. In our implementation, we truncate the spatial integral because data are, in practice, ac-

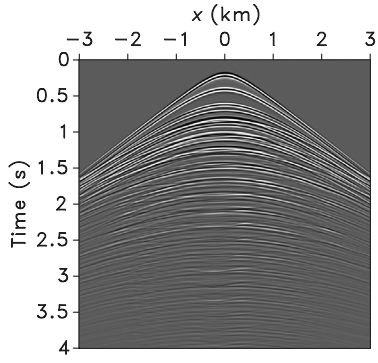

Figure 6. The reflection response corresponding to the inhomogeneous velocity and density model in Figures 4 and 5 with the source and receivers at the surface.

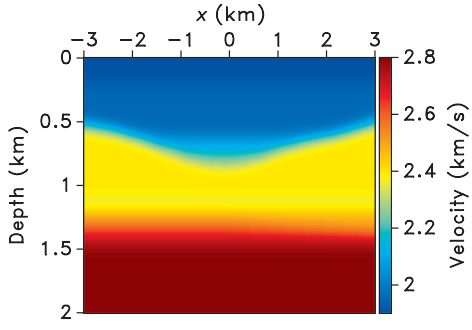

Figure 7. Macromodel, i.e., smooth version of Figure 4, used to compute the first arrivals from the virtual source location to the surface.

quired for a finite range of offsets. This truncation requires tapering at the edges of the reflection response, which corresponds to the reduced amplitudes of the focusing functions at the far offsets.

From iteration index $k = 0$ to $k = 1$, new events are generated in the focusing function. Even the focusing function $f^{-}_{1,k}$ at $k = 0$ already has the main features that are obtained after five iterations. In iteration $k = 1$ to $k = 5$, the focusing functions look kinematically similar. Higher order iterations generally correct the amplitude errors in the focusing functions.

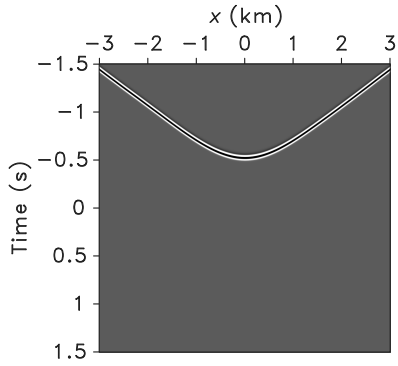

Figure 8. The time-reversed first arrival for a virtual source at $\mathbf{x_i} = (0, 1100)$ m and receivers at the surface. This event is used to initialize the Marchenko iterative scheme ($\mathcal{T}_d^{\text{inv}}$).

Green's function retrieval

By substituting the focusing functions in equations 14 and 15, we obtain the one-way pressure-normalized Green's functions, as shown in Figure 10. These up- and downgoing Green's functions are the response for a receiver at $\mathbf{x}_\mathbf{i}' = (0, 1100)$ m and variable source locations $\mathbf{x}_\mathbf{0}''$. To enhance the internal and free-surface multiples in Figure 10, we display Green's functions with a time-dependent gain of $\exp 1.5t$.

The two-way Green's function is given as the summation of the up- and downgoing Green's functions. A comparison of this retrieved two-way Green's function with the modeled Green's function (modeled with the exact small-scale variations in the velocity and density) is shown in Figure 11. Again, we apply a gain of $\exp\ 1.5t$ to Green's functions in Figure 11. The retrieved and modeled Green's functions match almost perfectly, as shown in Figure 11. As expected, the far offsets do not provide a good match; in particular, the recovered amplitudes are too low because we truncate the spatial integrals at the far offsets in the Marchenko equations.

Comparison of Green's functions with and without the free surface

The previous formulations of Green's function retrieval, mentioned in the "Introduction" section, require the reflection response without free-surface multiples. This means that an additional

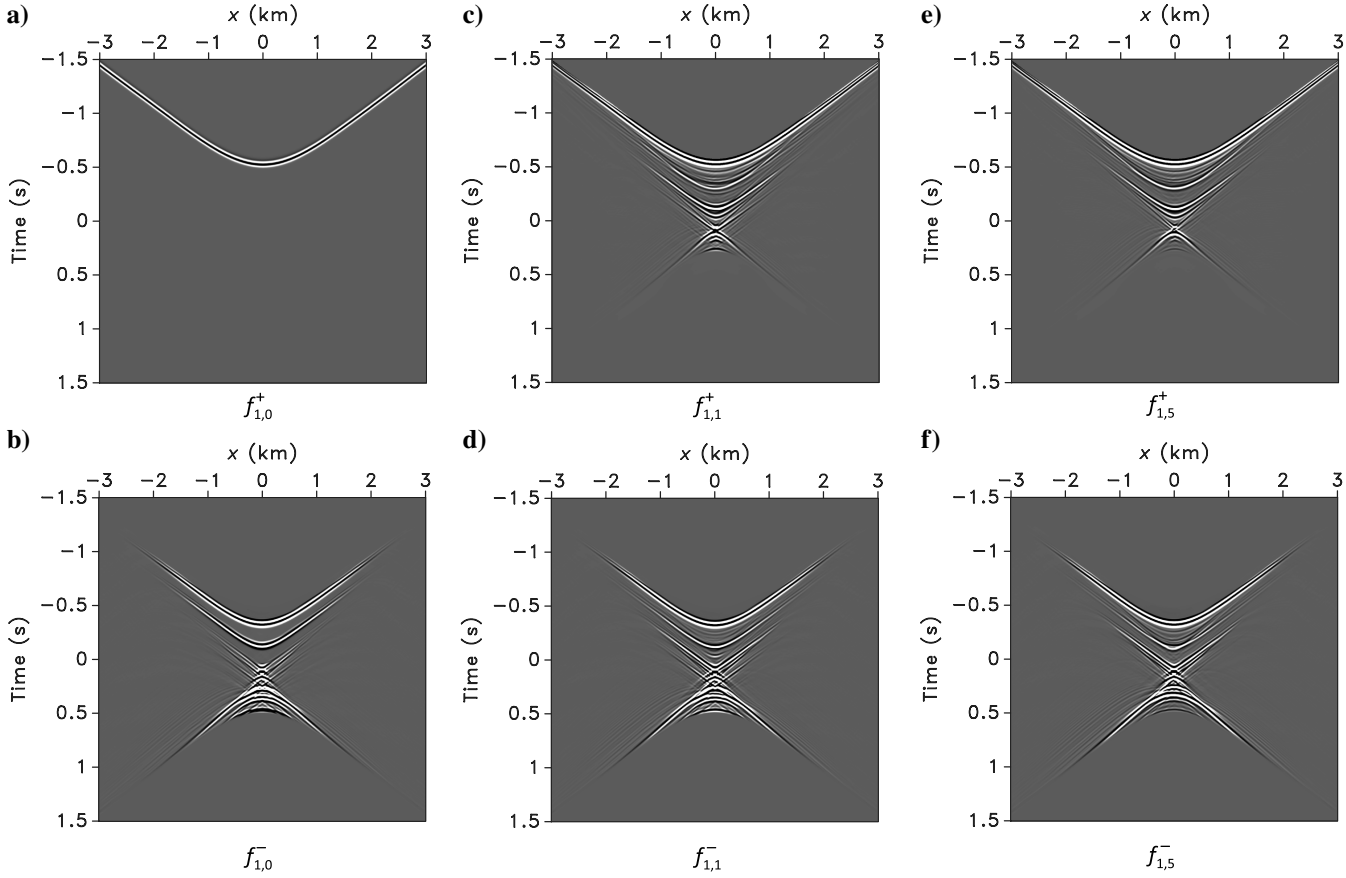

Figure 9. One-way focusing functions $f^{+}_{1,k}$ and $f^{-}_{1,k}$ that focus at $\mathbf{x}_\mathbf{i}'$ for iteration index $k = 0, 1, 5$.

processing step to remove the surface reflections is required before implementing the Green's function retrieval algorithm for past formulations. For such an implementation, the Green's function does not include free-surface multiples; hence, the imaging procedure does not take these multiples into account. Figure 12 shows the up- and downgoing one-way Green's function without free-surface multiples. Green's functions in Figure 12 are retrieved using the Marchenko method that does not take into account free-surface multiples (Broggini et al., 2014; Wapenaar et al., 2014a); we remove the free-surface multiples from the reflection response before retrieving these Green's functions.

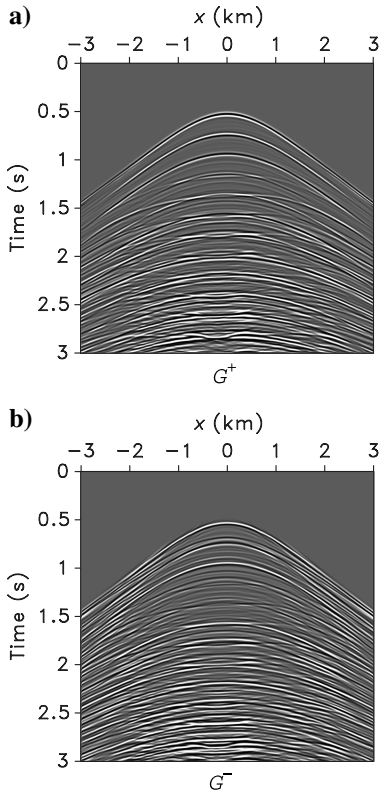

Figure 10. One-way pressure-normalized Green's functions G^+ (downgoing) and G^- (upgoing) for a virtual receiver position $\mathbf{x}_i' = (0, 1100)$ m and a range of source positions $\mathbf{x}_0''$. These Green's functions include free-surface multiples.

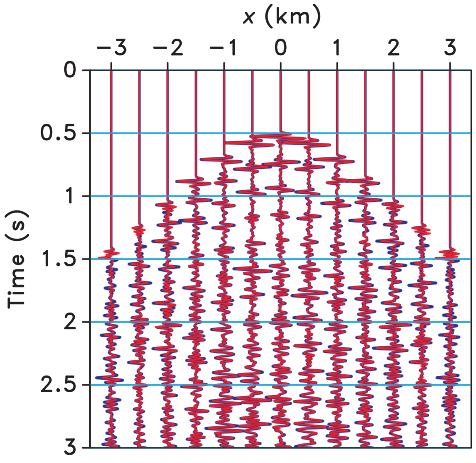

Figure 11. The retrieved two-way Green's function (in red) superimposed on the modeled Green's function (in blue, computed by finite differences with the small-scale details in the velocity and density model included) for a virtual receiver position $\mathbf{x}_i' = (0, 1100)$ m and a range of source positions $\mathbf{x}_0''$.

The Green's functions in Figure 12 are the response for a virtual receiver position $\mathbf{x}_i' = (0, 1100)$ m and variable source positions $\mathbf{x}_0''$. Here, a time-dependent gain of $\exp 1.5t$ is applied to the Green's functions. As expected, the Green's functions with the free surface G^+ and G^- have greater waveform complexity and higher amplitudes than the Green's functions in the absence of the free surface G_0^+ and G_0^-. This is obvious for times later than 1.5 s for Figures 10 and 12.

The events in the one-way Green's functions $G^\pm$ may be stronger than in $G_0^\pm$. For times later than 1 s, the free-surface multiples (in red) dominate in Figure 13. In addition, we avoid SRME on the reflection response using the Marchenko equations for Green's function retrieval that includes free-surface multiples (our work). It remains to be investigated to what extent these retrieved multiples improve the image quality.

Marchenko imaging — Target oriented

Ttarget-oriented Marchenko imaging entails retrieving the up- and downgoing Green's functions in the target area and using

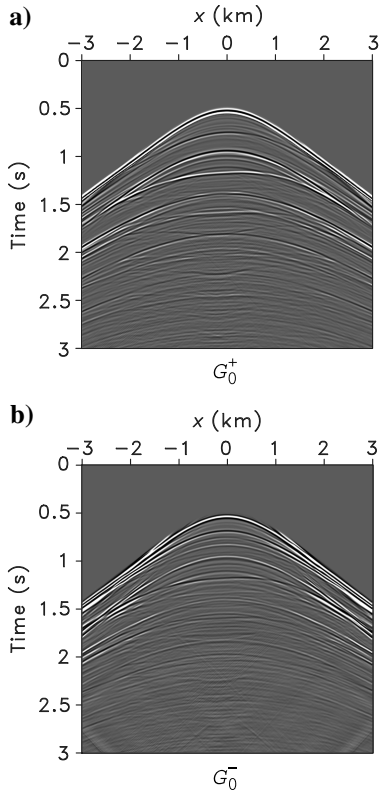

Figure 12. One-way pressure-normalized Green's functions G_0^+ (downgoing) and G_0^- (upgoing) for a virtual receiver position $\mathbf{x}_i' = (0, 1100)$ m and a range of source positions $\mathbf{x}_0''$. These Green's functions do not include free-surface multiples.

them to construct the target image in Figure 14. Figure 15 shows the Marchenko imaging of the model in Figure 14. To compute this image, we retrieve the up- and downgoing Green's functions $G^{\pm,q}(\mathbf{x}_\mathbf{i}', \mathbf{x}_\mathbf{0}'', t)$ at the virtual receiver locations $\mathbf{x}_\mathbf{i}' = (\mathbf{x}_\mathbf{H}', x_{3,i})$ ranging from $\mathbf{x}_{\mathbf{H},\mathbf{i}}' = -2$ to 2 km and $x_{3,i} = 1$ to 2 km. We sample $\mathbf{x}_{\mathbf{H},\mathbf{i}}'$ and $x_{3,i}$ every 40 and 10 m, respectively, to retrieve the Green's function. These functions are used to invert for $R_0(\mathbf{x}_\mathbf{i}, \mathbf{x}_\mathbf{i}', t)$ as explained in the "Theory" section. The contribution to the image is $R_0(\mathbf{x}_\mathbf{i}, \mathbf{x}_\mathbf{i}, 0)$, which is R_0 at zero offset and zero time for the range of $\mathbf{x}_\mathbf{i}$.

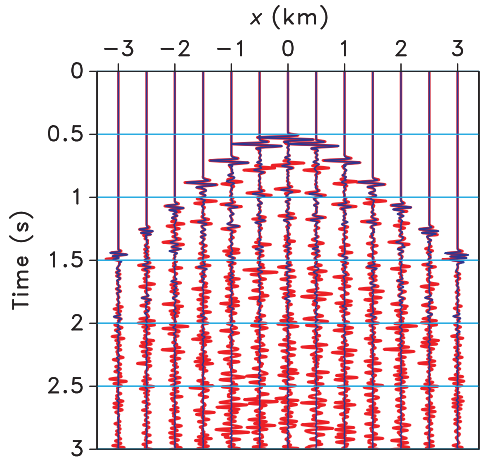

Figure 13. Green's function G_0 without the free surface (blue) and Green's function G with the free surface (red) for a virtual receiver at $\mathbf{x}_\mathbf{i}' = (0, 1100)$ m and a range of source positions $\mathbf{x}_\mathbf{0}''$.

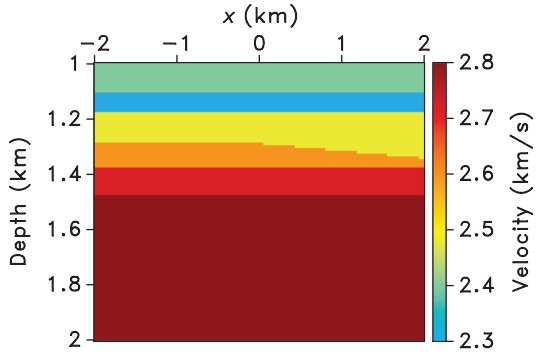

Figure 14. Region of the velocity model targeted for imaging. Note that we do not use this model to implement the Marchenko imaging; we use a smooth version of the velocity model (Figure 7) only. This model ranges from −2 to 2 km in the x_1-coordinate and 1–2 km in the x_3-coordinate.

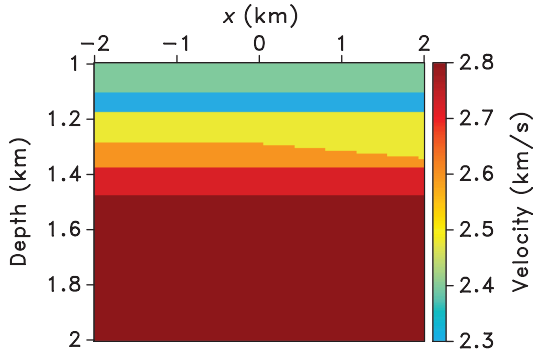

Figure 15. Target-oriented Marchenko imaging of the model in Figure 14 below the syncline structure. The image is $R_0(\mathbf{x}_\mathbf{i}, \mathbf{x}_\mathbf{i}, 0)$ for $\mathbf{x}_\mathbf{i}$ ranging from $\mathbf{x}_\mathbf{H} = -2$ to 2 km and $x_{3,i} = 1$ to 2 km.

The target-oriented Marchenko image, Figure 15, has its artifacts caused by the internal multiples and free-surface multiples in the overburden largely suppressed. If the free-surface multiples were incorrectly handled by Marchenko imaging, then the associated multiples caused by the syncline and the layers within the syncline would be present in our image. However, Marchenko imaging removes the artifacts related to the multiples caused by these interfaces, assuming sufficient aperture, and proper sampling (mentioned in this paper). To understand the adverse effects that the multiples have on the subsurface image, we show an reverse time migration image in Figure 16, which we know does not place multiples at the correct depth level. Only a magnified portion of the entire reverse time migrated image is shown in Figure 16, corresponding to the section containing the target location. Figure 16 includes many artifacts introduced by the multiples such that the actual reflectors in the model are masked by these artifacts.

We also remove the free surface from the reflection response and again conduct reverse time migration, as shown in Figure 17. Note that the reverse time migration image still has artifacts because the

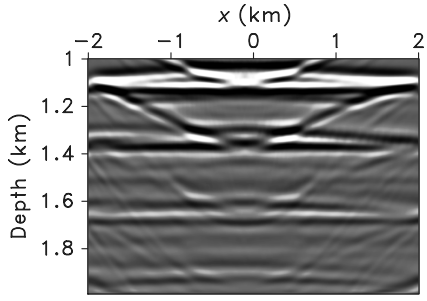

Figure 16. Magnified portion of the reverse time migrated image for the model in Figure 14 below the syncline structure. The surface reflection response used for imaging includes primaries, internal multiples, and free-surface multiples.

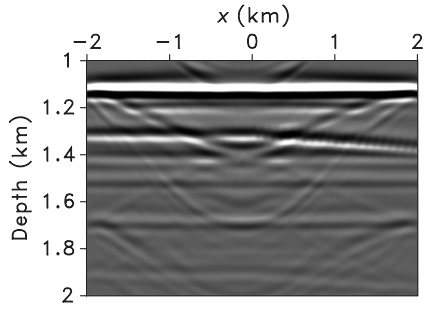

Figure 17. Magnified image of the reverse time migration for the model in Figure 14 below the syncline structure. The surface reflection response used for imaging includes primaries and internal multiples, and the free-surface multiples are removed.

reflection response has internal multiples that are not correctly handled by reverse time migration. These artifacts can be seen by comparing the target model in Figure 14 with the reverse time migration examples. The artifacts are either nonexistent or minimal in the target-oriented Marchenko imaging, as shown in Figure 15.

CONCLUSION

We have shown that we can retrieve the Green's function at any location in the subsurface without any knowledge of the small-scale variations of the subsurface once we have sufficient aperture coverage on the surface over the virtual source location. These Green's functions include not only primaries and internal multiples but also free-surface multiples. To retrieve the Green's function, we require the reflection response at the surface and a macromodel of the subsurface overburden velocity (at least between the surface and the virtual source depth level). In comparison to previous work on the Green's function retrieval by the Marchenko equation, our reflection response at the surface includes free-surface multiples, and therefore, it obviates the need to remove free-surface multiples in the reflection response.

The reflection response is required to be well-sampled at the surface. Such as in standard (primary) wavefield extrapolation methods, the accuracy of our Green's function retrieval depends on the kinematic accuracy of the macromodel. Note, however, that the recovery of multiples in the Green's function is not negatively affected by moderate errors in the macromodel. Another assumption of the Green's function retrieval scheme, in our present implementation, is that all waves can be decomposed into up- and downgoing events; hence, horizontally propagating waves are not included in our current method.

Once we know the Green's function at the surface and the virtual receiver locations, we should be able to infer the properties inside the medium (volume). We can form an image in two ways: (1) downward continuation of the reflection response to a given reference level at the top of the target zone and then performing conventional imaging in the target and (2) target-oriented imaging at all depth levels in the target. In this paper, we follow the second approach. We construct a target-oriented image by deconvolution of the up- and downgoing Green's functions, evaluated at zero offset and zero time for all depth levels in the target.

In the numerical examples, we observe no significant artifacts in the Marchenko image due to misplaced multiples, even though the reflection response includes multiples (no preprocessing is done to remove the multiples). How the multiples can improve the image is yet to be investigated; however, Marchenko imaging largely suppresses the artifacts caused by internal and free-surface multiples.

Significantly, the inputs for Marchenko imaging and the current state-of-the-art imaging techniques are the same: the reflection response and a macromodel. However, in Marchenko imaging, we accurately handle not only the primaries but also the multiples.

ACKNOWLEDGMENTS

This work was funded by the sponsor companies of the Consortium Project on Seismic Inverse Methods for Complex Structures. We are grateful to D. Witters for her help in preparing this manuscript and I. Vasconcelos (Schlumberger Gould Research), E. Diaz (CWP), and V. Li (CWP) for fruitful discussions. The numeric examples in this paper are generated with the Madagascar open-source software package freely available from http://www.ahay.org. We would also like to thank our reviewers: F. Broggini, C. A. da Costa Filho, J. Shragge, and an anonymous reviewer for their valuable suggestions. The 2D reflection response in this paper is generated with the finite-difference package in Thorbecke and Draganov (2011).

REFERENCES

Amundsen, L., 2001, Elimination of free-surface related multiples without need of the source wavelet: Geophysics, **66**, 327–341, doi: 10.1190/1.1444912.

Behura, J., K. Wapenaar, and R. Snieder, 2014, Autofocus Imaging: Image reconstruction based on inverse scattering theory: Geophysics, **79**, no. 3, A19–A26, doi: 10.1190/geo2013-0398.1.

Berkhout, A., and D. Verschuur, 1997, Estimation of multiple scattering by iterative inversion. Part I: Theoretical considerations: Geophysics, **62**, 1586–1595, doi: 10.1190/1.1444261.

Berkhout, A., and D. Verschuur, 2006, Imaging of multiple reflections: Geophysics, **71**, no. 6, SI209–SI220, doi: 10.1190/1.2215359.

Broggini, F., R. Snieder, and K. Wapenaar, 2012, Focusing the wavefield inside an unknown 1D medium: Beyond seismic interferometry: Geophysics, **77**, no. 5, A25–A28, doi: 10.1190/geo2012-0060.1.

Broggini, F., R. Snieder, and J. Wapenaar, 2014, Data-driven wavefield focusing and imaging with multidimensional deconvolution: Numerical examples for reflection data with internal multiples: Geophysics, **79**, no. 3, WA107–WA115, doi: 10.1190/geo2013-0307.1.

Claerbout, J., 1971, Toward a unified theory of reflector mapping: Geophysics, **36**, 467–481, doi: 10.1190/1.1440185.

da Costa Filho, C. A., and A. Curtis, 2015, Elastic P- and S-wave autofocus imaging with primaries and internal multiples: Geophysics, **80**, no. 5, S187–S202, doi: 10.1190/geo2014-0512.1.

da Costa Filho, C. A., M. Ravasi, A. Curtis, and G. A. Meles, 2014, Elastodynamic Green's function retrieval through single-sided Marchenko inverse scattering: Physical Review E, **90**, 063201, doi: 10.1103/PhysRevE.90.063201.

Guitton, A., 2002, Shot-profile migration of multiple reflections: 72nd Annual International Meeting, SEG, Expanded Abstracts, 1296–1299.

Jiang, Z., J. Sheng, J. Yu, G. Schuster, and B. Hornby, 2007, Migration methods for imaging different-order multiples: Geophysical Prospecting, 19–1 ,**55**, doi: 10.1111/j.1365-2478.2006.00598.x.

Lokshtanov, D., 1999, Multiple suppression by data-consistent deconvolution: The Leading Edge, **18**, 115–119, doi: 10.1190/1.1438136.

Malcolm, A., B. Ursin, and V. Maarten, 2009, Seismic imaging and illumination with internal multiples: Geophysical Journal International, **176**, 847–864, doi: 10.1111/j.1365-246X.2008.03992.x.

Muijs, R., J. O. A. Robertsson, and K. Holliger, 2007a, Prestack depth migration of primary and surface-related multiple reflections: Part I: Imaging: Geophysics, **72**, no. 2, S59–S69, doi: 10.1190/1.2422796.

Muijs, R., J. O. A. Robertsson, and K. Holliger, 2007b, Prestack depth migration of primary and surface-related multiple reflections: Part II: Identification and removal of residual multiples: Geophysics, **72**, no. 2, S71–S76, doi: 10.1190/1.2424544.

Ong, C., C. Lapilli, J. Perdomo, and R. Coates, 2002, Extended imaging and illumination in wave migrations: 72nd Annual International Meeting, SEG, Expanded Abstracts, 4116–4120.

Ramírez, A., and A. Weglein, 2005, An inverse scattering internal multiple elimination method: Beyond attenuation, a new algorithm and initial tests: 75th Annual International Meeting, SEG, Expanded Abstracts, 2115–2118.

Reiter, E., M. Toksöz, T. Keho, and G. Purdy, 1991, Imaging with deep-water multiples: Geophysics, **56**, 1081–1086, doi: 10.1190/1.1443119.

Rose, J., 2002a, Single-sided autofocusing of sound in layered materials: Inverse problems, **18**, 1923–1934, doi: 10.1088/0266-5611/18/6/329.

Rose, J., 2002b, Time reversal, focusing and exact inverse scattering, *in* M. Fink, W. A. Kuperman, J.-P. Montagner, and A. Tourin, eds., Imaging of complex media with acoustic and seismic waves: Springer, 97–106.

Schuster, G. T., Z. Jiang, and J. Yu, 2003, Imaging the most bounce out of multiples: 65th Annual International Conference and Exhibition, EAGE, Extended Abstracts, session on Multiple Elimination.

Singh, S., R. Snieder, J. Behura, J. van der Neut, K. Wapenaar, and E. Slob, 2015, Marchenko imaging: Imaging with primaries, internal multiples, and free-surface multiples: Geophysics, **80**, no. 5, S165–S174, doi: 10.1190/geo2014-0494.1.

Slob, E., K. Wapenaar, F. Broggini, and R. Snieder, 2014, Seismic reflector imaging using internal multiples with Marchenko-type equations: Geophysics, **79**, no. 2, S63–S76, doi: 10.1190/geo2013-0095.1.

Thorbecke, J. W., and D. Draganov, 2011, Finite-difference modeling experiments for seismic interferometry: Geophysics, **76**, no. 6, H1–H18, doi: 10.1190/geo2010-0039.1.
Ursin, B., 1983, Review of elastic and electromagnetic wave propagation in horizontally layered media: Geophysics, **48**, 1063–1081, doi: 10.1190/1.1441529.
van der Neut, J., J. Thorbecke, K. Mehta, E. Slob, and K. Wapenaar, 2011, Controlled-source interferometric redatuming by crosscorrelation and multidimensional deconvolution in elastic media: Geophysics, **76**, no. 4, SA63–SA76, doi: 10.1190/1.3580633.
van Groenestijn, G., and D. Verschuur, 2009, Estimating primaries by sparse inversion and application to near-offset data reconstruction: Geophysics, **74**, no. 3, A23–A28, doi: 10.1190/1.3111115.
Verschuur, D., and A. Berkhout, 2005, Removal of internal multiples with the common- focus-point (CFP) approach: Part 2. Application strategies and data examples: Geophysics, **70**, no. 3, V61–V72, doi: 10.1190/1.1925754.
Verschuur, D., A. Berkhout, and C. Wapenaar, 1992, Adaptive surface-related multiple elimination: Geophysics, **57**, 1166–1177, doi: 10.1190/1.1443330.
Wapenaar, K., 1998, Reciprocity properties of one-way propagators: Geophysics, **63**, 1795–1798, doi: 10.1190/1.1444473.
Wapenaar, K., 2014, Single-sided Marchenko focusing of compressional and shear waves: Physical Review E, **90**, 063202, doi: 10.1103/PhysRevE.90.063202.
Wapenaar, K., F. Broggini, E. Slob, and R. Snieder, 2013, Three-dimensional single-sided Marchenko inverse scattering, data-driven focusing, Green's function retrieval, and their mutual relations: Physical Review Letters, **110**, 084301, doi: 10.1103/PhysRevLett.110.084301.
Wapenaar, K., F. Broggini, and R. Snieder, 2011, A proposal for model-independent 3D wavefield reconstruction from reflection data: 81st Annual International Meeting, SEG, Expanded Abstracts, 3788–3792.
Wapenaar, K., J. Fokkema, M. Dillen, and P. Scherpenhuijsen, 2000, One-way acoustic reciprocity and its applications in multiple elimination and time-lapse seismics: 70th Annual International Meeting, SEG, Expanded Abstracts, 2377–2380.
Wapenaar, C. P. A., and J. L. T. Grimbergen, 1996, Reciprocity theorems for one-way wavefields: Geophysical Journal International, **127**, 169–177, doi: 10.1111/j.1365-246X.1996.tb01542.x.
Wapenaar, C., G. Peels, V. Budejicky, and A. Berkhout, 1989, Inverse extrapolation of primary seismic waves: Geophysics, **54**, 853–863, doi: 10.1190/1.1442714.
Wapenaar, K., and E. Slob, 2014, On the Marchenko equation for multicomponent single-sided reflection data: Geophysical Journal International, **199**, 1367–1371, doi: 10.1093/gji/ggu313.
Wapenaar, K., E. Slob, and R. Snieder, 2008, Seismic and electromagnetic controlled-source interferometry in dissipative media: Geophysical Prospecting, **56**, 419–434, doi: 10.1111/j.1365-2478.2007.00686.x.
Wapenaar, K., J. Thorbecke, J. van der Neut, F. Broggini, E. Slob, and R. Snieder, 2014a, Green's function retrieval from reflection data, in absence of a receiver at the virtual source position: Journal of the Acoustical Society of America, **135**, 2847–2861, doi: 10.1121/1.4869083.
Wapenaar, K., J. Thorbecke, J. van der Neut, F. Broggini, E. Slob, and R. Snieder, 2014b, Marchenko imaging: Geophysics, **79**, no. 3, WA39–WA57, doi: 10.1190/GEO2013-0302.1.
Weglein, A., F. Araújo, P. Carvalho, R. Stolt, K. Matson, R. Coates, D. Corrigan, D. Foster, S. Shaw, and H. Zhang, 2003, Inverse scattering series and seismic exploration: Inverse problems, **19**, R27–R83, doi: 10.1088/0266-5611/19/6/R01.
Weglein, A., F. Gasparotto, P. Carvalho, and R. Stolt, 1997, An inverse-scattering series method for attenuating multiples in seismic reflection data: Geophysics, **62**, 1975–1989, doi: 10.1190/1.1444298.
Wiggins, J., 1988, Attenuation of complex water-bottom multiples by wave-equation-based prediction and subtraction: Geophysics, **53**, 1527–1539, doi: 10.1190/1.1442434.
Ypma, F., and D. Verschuur, 2013, Estimating primaries by sparse inversion, a generalized approach: Geophysical Prospecting, **61**, 94–108, doi: 10.1111/j.1365-2478.2012.01095.x.
Ziolkowski, A., D. Taylor, and R. Johnston, 1999, Marine seismic wavefield measurement to remove sea-surface multiples: Geophysical Prospecting, **47**, 841–870, doi: 10.1046/j.1365-2478.1999.00165.x.